Influence of Ground Clutter Contamination on Polarimetric Radar Parameters

KATJA FRIEDRICH* AND URS GERMANN

MeteoSvizzera, Locarno, Switzerland

PIERRE TABARY

Direction des Systèmes d'Observation, Centre de Météorologie Radar, Météo-France, Trappes, France

(Manuscript received 16 November 2007, in final form 24 July 2008)

ABSTRACT

The influence of ground clutter contamination on the estimation of polarimetric radar parameters, horizontal reflectivity (Z_h), differential reflectivity (Z_{dr}), correlation coefficient (ρ_{hv}), and differential propagation phase (ϕ_{dp}) was examined. This study aims to derive the critical level of ground clutter contamination for Z_h, Z_{dr}, ρ_{hv}, and ϕ_{dp} at which ground clutter influence exceeds predefined precision thresholds. Reference data with minimal ground clutter contamination consist of eight precipitation fields measured during three rain events characterized by stratiform and convective precipitation. Data were collected at an elevation angle of 0.8° by the Météo-France operational, polarimetric Doppler C-band weather radar located in Trappes, France, ~30 km southwest of Paris. Nine different ground clutter signatures, ranging from point targets to more complex signatures typical for mountain ranges or urban obstacles, were added to the precipitation fields. This is done at the level of raw in-phase and quadrature component data in the two polarimetric channels. For each ground clutter signature, 30 simulations were conducted in which the mean reflectivity of ground clutter within the resolution volume varied between being 30 dB higher to 30 dB lower than the mean reflectivity of precipitation. Differences in Z_h, Z_{dr}, ρ_v, and ϕ_{dp} between simulation and reference were shown as a function of ratio between ground clutter and precipitation intensities.

As a result of this study, horizontal reflectivity showed the lowest sensitivity to ground clutter contamination. Furthermore, a precision of 1.7 dBZ in Z_h is achieved on average when the precipitation and ground clutter intensities are equal. Requiring a precision of 0.2 dB in Z_{dr} and 3° in ϕ_{dp}, the reflectivity of precipitation needs to be on average ~5.5 and ~6 dB, respectively, higher compared to the reflectivity of ground clutter. The analysis also indicates that the highest sensitivity to the nine clutter signatures was derived for ρ_{hv}. To meet a predefined precision threshold of 0.02, reflectivity of precipitation needs to be ~13.5 dB higher than the reflectivity of ground clutter.

1. Introduction

Many studies have focused on investigating benefits of radar polarimetry for operational applications (e.g., Zrnic and Ryzhkov 1996; Zrnic and Ryzhkov 1999; Bringi and Chandrasekar 2001; Illingworth 2003; Sugier and Tabary 2006; Gourley et al. 2007a,b). They concluded that polarimetry is primarily useful for identifying nonmeteorological echoes; classifying hydrometeors in particular snow, hail, and graupel; correcting data for attenuation and beam shielding; and quantifying rainfall rates, especially in heavy rain. Based on these results, many weather services have already decided to upgrade their current operational weather radar network to have dual-polarization capability.

Conventional single-polarization Doppler weather radars obtain reflectivity at horizontal polarization (Z_h) and Doppler velocity. Most dual-polarization radars simultaneously transmit and receive horizontally and vertically polarized waves (referred to as hybrid mode). In addition to reflectivity, dual-polarization radars derive the ratio of horizontal to vertical reflectivity or differential reflectivity (Z_{dr}), correlation coefficient (ρ_{hv}) computed from the power received at horizontal and vertical

* Current affiliation: Department of Atmospheric and Oceanic Sciences, University of Colorado at Boulder, Boulder, Colorado.

Corresponding author address: Dr. Katja Friedrich, ATOC, University of Colorado at Boulder, UCB 311, Boulder, CO 80309-0311.
E-mail: katja.friedrich@colorado.edu

DOI: 10.1175/2008JTECHA1092.1

polarizations, and phase difference between horizontally and vertically polarized returns or differential propagation phase (ϕ_{dp}). Dual-polarization radars that transmit and receive horizontally and vertically polarized waves at an alternating mode can additionally derive the ratio between horizontally transmitted/vertically received reflectivity and horizontal reflectivity or linear depolarization ratio (L_{dr}).

Large numbers of studies have shown that the quality of radar products in mountainous terrain will increase significantly by using polarimetric information because of a better clutter identification and usage of phase measurements within areas of strong radar beam shielding (Zrnic and Ryzhkov 1996; Vivekanandan et al. 1999; Gourley et al. 2007b). However, only a few studies have addressed the influence of ground clutter on the quality of polarimetry so far (e.g., Blackman and Illingworth 1993; Zrnic and Ryzhkov 1996; Vivekanandan et al. 1999; Illingworth 2003; Giangrande and Ryzhkov 2005; Friedrich et al. 2007). Although it is widely known that ground clutter has a stronger impact on the precision of polarimetric measurements compared to radar reflectivity, it has never been quantified objectively based on real measurements. Illingworth (2003) quantified theoretically the impact of random phase of ground clutter on the precision of ϕ_{dp} measurements. He indicated that a superposition of random phase of ground clutter with precipitation having an amplitude 10 times larger will lead to a phase noise of 5°. The study presented here is unique because it is the first analysis that objectively quantifies the relation between ground clutter and signal echoes for all polarimetric quantities based on real measurements.

Why is this quantification important? First, clutter correction can become computationally expensive, time consuming, and prone to failure (removing weather instead of ground clutter signal). Most of the latest clutter correction techniques (e.g., spectral techniques) have not been tested for polarimetric measurements and staggered pulse repetition frequencies (PRFs)—a technique becoming widely used to overcome the Doppler-range dilemma in operational services. Operational weather radars mostly identify and remove instead of correcting for ground clutter (Lee et al. 1995; Gourley et al. 2007b). To implement the latest clutter correction techniques operationally (less computationally expensive and time consuming), they could be applied selectively within areas that can be located with a quantification of the clutter to signal strength in relation to the measurement precision. The quantification of the quality of the measurement might help to identify areas where the quality of polarimetric measurements is sufficiently high to use them for further applications. Most clutter contamination caused by the interaction between the main lobe of the transmitted power pattern and obstacles can be detected using convectional methods and polarimetric clutter filters. By superimposing weak clutter and strong weather signatures (e.g., in the case of sidelobe contamination), the typical signatures in reflectivity and polarimetry might become weak and hard to detect.

Because mountains and urban obstacles modify each individual transmitted radar pulse through main and side lobes, the potential impact of these contaminations on the measurement precision of Z_{dr}, ϕ_{dp}, and ρ_{hv}, which are averaged over several radar pulses, needs to be carefully assessed before making a decision on what kind of ground clutter concept needs to be applied to a future Swiss polarimetric weather radar network. Figure 1 shows the maximum reflectivity within a vertical column (composite reflectivity) of 1 km $\times$ 1 km base area ranging from the ground to 12 km MSL, measured by the three weather radars operated by the Swiss weather service (MeteoSwiss). No precipitation was reported and measured over the Alps on that day so that return in the radar image can be related to mountain returns and urban obstacles. Currently, ground clutter shown in Fig. 1 is reduced by oversampling using high-range-resolution (83 m) seeking for clutter-free returns among the 12 measurements within the 1-km range interval. Clutter is effectively eliminated by using the seven-step clutter elimination algorithm of Joss and Lee (1995) and Germann et al. (2006). In the following study, we specifically focus on dual-polarization radars operating in the hybrid mode; that is, precision of L_{dr} is not considered.

This study is unique in the sense that we determine the critical level of ground clutter contamination for Z_h, Z_{dr}, ρ_{hv}, and ϕ_{dp} at which ground clutter influence exceeds predefined accuracy. Special emphasis is placed on those cases in which ground clutter intensity is much lower than that of precipitation to simulate, specifically, the impact of sidelobe contamination on the precision needed in polarimetric variables. This is often the case when antenna side lobes hit urban obstacles or mountains that contribute additionally but with lower intensity to the signals coming from the antenna main lobe. To monitor the difference between precipitation and ground clutter intensity, the instantaneous precipitation within areas of minimum influence from obstacles and the reflectivity of obstacle returns within optical clear air are superimposed. The emphasis of this study is to derive the critical level (difference between precipitation and ground clutter) when measurements of Z_{dr}, ρ_{hv}, and ϕ_{dp} will have a minimum precision required for most applications (e.g., rainfall rate estimation, hydrometeor classification). The application of various ground clutter filters to this analysis

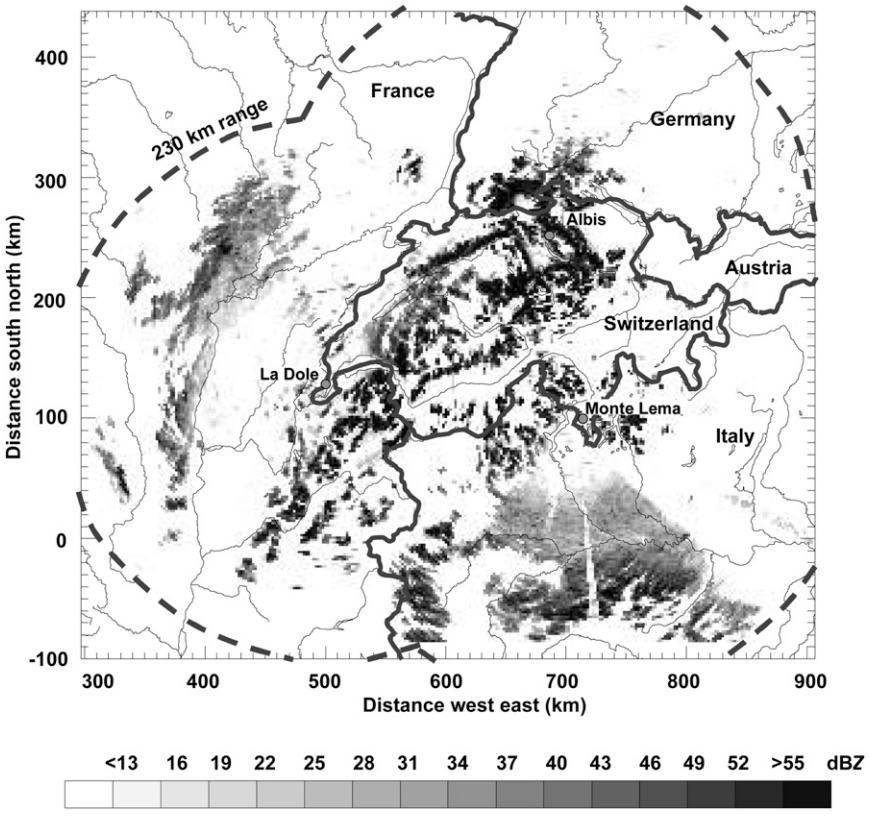

FIG. 1. Maximum reflectivity (dBZ) within a vertical column of 1 km × 1 km base area ranging from the ground to 12 km MSL. Measurements were obtained at 1300 UTC 18 Mar 2003 by the three weather radars Albis, La Dole, and Monte Lema operated by the Swiss Weather Service. Measurements were accomplished within a range of 230 km around the radar indicated by dashed gray lines. On that day the Alps were free of precipitation so that the returns were primarily caused by mountains and obstacles at ground level. Country borders are indicated as thick solid gray lines. Operational clutter elimination was switched off.

is beyond the scope of the paper due to the large number of ground clutter concepts. Most of them are often tied closely to the main applications (hydrology, nowcasting, rainfall-rate estimation, data assimilation, research) leading to various hardware setups (e.g., staggered dual/triple PRF, oversampling, choice of PRT defining the maximum range, age of the signal processor).

Observing systems and characteristics of the studied precipitation events are described in section 2, while the analysis methodology is presented in section 3. The sensitivity of polarimetric parameters to ground clutter is discussed in section 4. Finally, conclusions are summarized in section 5.

2. Observing system and measuring data

a. Observing system

Because present MeteoSwiss weather radars are only single polarized, the analysis was conducted with data measured by the polarimetric C-band Doppler radar located at Trappes, France, which is located ~30 km southwest of Paris. It is operated by the French weather service (Météo-France) and is part of the operational weather radar network (Parent du Châtelet et al. 2005; Tabary 2007). Transmitted frequency is 5.64 GHz, resulting in a wavelength of 5.31 cm. Beamwidth is equal to 1.1°. This polarized radar was designed to simultaneously transmit and receive horizontally and vertically polarized waves. The transmission is accomplished at three different pulse repetition frequencies (referred to as triple-PRF scheme) with 379, 325, and 303 Hz to overcome difficulties in dealiasing Doppler velocities (Tabary et al. 2007). The mean PRF is equal to 333 Hz. The Météo-France signal processor is capable of storing time series of the in-phase (I) and quadrature (Q) components of the complex radar signal during its operation. During data collection, the antenna was scanning at a velocity of ~6° s^{-1} (~1 revolution per minute).

TABLE 1. Threshold and dynamic range of variables for defining areas of precipitation. Texture expresses the spatial variability of Z_{dr} and is computed by determining the mean between the differences between three pixels in azimuth direction and three along the range centered on the gate (Gourley et al. 2007b). Beam shielding was derived considering the influence of topography and urban obstacles in the vicinity (for more information, see Friedrich et al. 2007).

Variable	Thresholds/dynamic range
Range	$25 <$ range < 100 km
Z_h	$15 < Z_h < 50$ dBZ
Z_{dr}	Texture(Z_{dr}) < 1.5
	$0 < Z_{dr} < 4$ dB
ρ_{hv}	> 0.97
ϕ_{dp}	$< 20°$
Beam shielding	$< 50\%$

To be consistent with the standard spatial resolution of dual-polarization products of Météo-France (azimuth-range resolution of 0.5° × 240 m) and the mean PRF, the radar parameters were derived from 27 successive signal samples (I and Q measures).

b. Precipitation data

The analysis was conducted by using data from eight analysis times, which were recorded during three precipitation events. One analysis time consists of measurements that were obtained from a single 360° scan at an elevation angle of 0.8°. The analysis concentrated solely on those pixels that show polarimetric signatures typical for precipitation. Pixels that contained non-precipitating particles and those that were affected by attenuation based on thresholds for polarimetric variables listed in Table 1 were removed. Based on quality control and flat topography around Trappes, these reference precipitation fields are assumed to have minor contamination related to mountains and urban obstacles.

Precipitation and polarimetric characteristics based on radar data for each analysis time are listed in Table 2. Precipitation samples were taken in October and November with mainly stratiform precipitation and some areas of enhanced precipitation observed in the afternoon on 3 October (Table 2; area with >25 mm h^{-1}). Precipitation characteristics vary only slightly from case to case with respect to average precipitation distribution and polarimetric quantities. On 15 November 2005, a wide cold-frontal rainband moved from north-northwest into the observational domain between 1436 and 1456 UTC. Precipitation was mainly located in the northern part of the observational domain, which was limited to a radius of 100 km around the radar. About 33% of this area had rainfall rates of ≥1 mm h^{-1} (corresponding to $Z_h > 24$ dBZ in Table 2). Within 20 min the area with rainfall rates ≥10 mm h^{-1} (corresponding to $Z_h > 46$ dBZ in Table 2) slightly increased, covering 0.6% of the 100-km range at 1436 UTC to 1.6% at 1456 UTC. On 2 October 2006, a warm-frontal rainband crossed the observational domain from the west-southwest, followed by a wide cold-frontal rainband passing the observational domain from the west on 3 October 2006. At 1223 UTC 2 October, ~20.8% (0.2%) of the observational domain had rainfall rates of ≥1 mm h^{-1} (≥10 mm h^{-1}), which was scattered mainly in the western, southern, and eastern parts of the observational domain. On 3 October, the cold-frontal rainband moved into the observational domain in the morning hours and the area of precipitation with ≥1 mm h^{-1} enlarged from about 18% to 26% between 0916 and 1356 UTC. The area of more intense rainfall (≥10 mm h^{-1}) also increased with time from 0.9% to 4.5%. The mean reflectivity within rain was slightly higher during the passage of the cold-frontal rainband with 26–30 dBZ (Table 2) compared to mean reflectivity observed on 2 October (22 dBZ). Mean Z_{dr} was ~0.3 dB on 2 and 3

TABLE 2. Areal coverage of precipitation with $Z_h > 24$ dBZ (> 1 mm h^{-1}) and $Z_h > 46$ dBZ (> 25 mm h^{-1}), mean horizontal reflectivity $\overline{Z_h}$, differential reflectivity $\overline{Z_{dr}}$, and correlation coefficient $\overline{\rho_{hv}}$ averaged over 360° in azimuth and 100-km range from the radar for data conducted at 0.8° elevation on 15 Nov 2005 and 2 and 3 Oct 2006.

Analysis time (UTC)	Area of $Z_h > 24$ dBZ (%)	Area of $Z_h > 46$ dBZ (%)	$\overline{Z_h}$ (dBZ)	$\overline{Z_{dr}}$ (dB)	$\overline{\rho_{hv}}$
		15 Nov 2005			
1436	32.6	0.6	29.1	0.49	0.99
1446	33.9	0.9	29.7	0.50	0.99
1456	34	1.6	30.3	0.53	0.99
		2 Oct 2006			
1223	20.8	0.2	21.6	0.28	0.99
		3 Oct 2006			
0916	17.6	0.9	26.9	0.34	0.99
1226	15.7	0.3	21.7	0.32	0.99
1352	26.7	4.2	25.6	0.28	0.99
1356	25.6	4.5	25.1	0.28	0.98

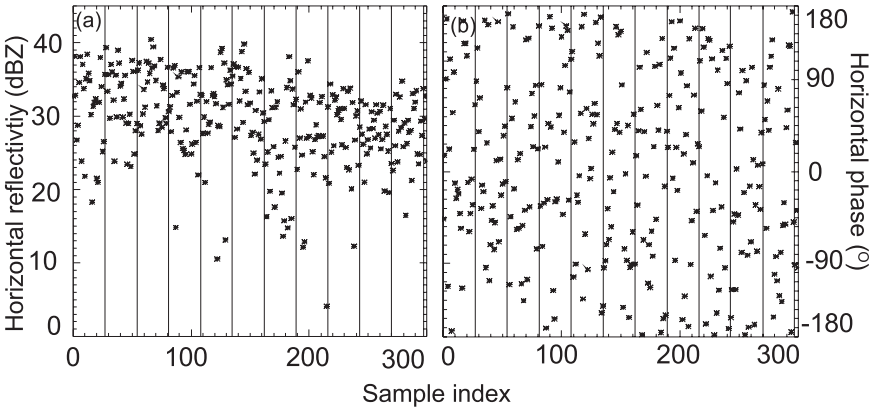

FIG. 2. Distribution of (a) horizontal reflectivity and (b) horizontal phase angle of moving scatterers primarily related to rain along an azimuthal interval of ~5.5° at 67.4-km range at 1451 UTC 15 Nov 2005. Each symbol represents an I and Q measurement at horizontal polarization. For an azimuthal resolution of 0.5° indicated by thin vertical lines, 27 successive samples were averaged.

October, while higher-mean Z_{dr} values observed on 15 November indicated the existence of larger raindrops. During all analysis times, ρ_{hv} showed values (~0.99) typically observed within rain. Measurements at 0.8° elevation angle and 100-km maximum range were conducted below the melting layer during all events.

Generally, hydrometeors are nonuniformly distributed within a sample volume. Because the number of hydrometeors can be large during precipitation events and their position relative to the radar is random, the independent in-phase and quadrature component measurements are random Gaussian distributed (Doviak and Zrnic 1993). Figure 2 shows reflectivity and phase angle derived from each individual signal sample (I and Q measures) from the horizontal polarization channel observed within rain. The sample volume was mainly filled with small spherical raindrops as indicated by $\rho_{hv} = 0.99$ and $Z_{dr} = 0.4$ dB, derived from 27 signal samples in the horizontal and vertical channel.

c. Ground clutter data

Contrary to precipitation samples, I and Q components of obstacles reveal a distinct signature in reflectivity and phase angle. The signature of the patterns depends strongly on the sum of all obstacles within the resolution volume, distance from the radar, antenna speed, and transmitted antenna power pattern. The I and Q samples of isolated obstacles approximately resample the transmitted antenna power and phase angle pattern. Although the antenna transmits and receives its main power through the main lobe (~1.1° in this case), power with lower intensity is also transmitted off the main beam through side lobes. If many obstacles with numerous exterior right angles are clustered together, the transmitted intensity through the side lobes, for instance, can even be intensified. To mimic the influence of different types of obstacles on the measurement precision, various I and Q samples located at different ranges from the radar resembling different parts of the transmitted antenna beam pattern were extracted from clear-air measurements. Figure 3 shows reflectivity and phase angle at horizontal polarization of nine samples from urban obstacles that were chosen for this study. Because the analysis presented here is computationally expensive (section 3), the study is limited to nine samples. The variation of the results depending on the type of ground clutter is explicitly discussed in section 4b.

The number of successive samples varied from 45 samples (Fig. 3a) to 119 samples (Fig. 3c) to imitate the variations in reflectivity and phase for different ground clutter types (cf. Figs. 3a,h). A part of the main lobe of the antenna beam (~0.8° in azimuth) is represented in Fig. 3a when the radar scanned across the Eiffel Tower in Paris. Main and secondary lobes of the power and phase angle pattern are shown in Fig. 3c. Comparisons between I and Q samples of isolated urban obstacles (towers) and isolated mountains showed a very similar backscattering pattern (figures not shown). Generally, nonmoving targets have the same spectral signature with power at zero velocity. Urban obstacles might be more prone to movement related, for instance, to tree foliage moving with the wind, swaying buildings, etc. Therefore, it can be hypothesized that the results of this analysis conducted with urban obstacles also apply in a similar way for mountains. More complex patterns of the backscattered power and phase resembling the

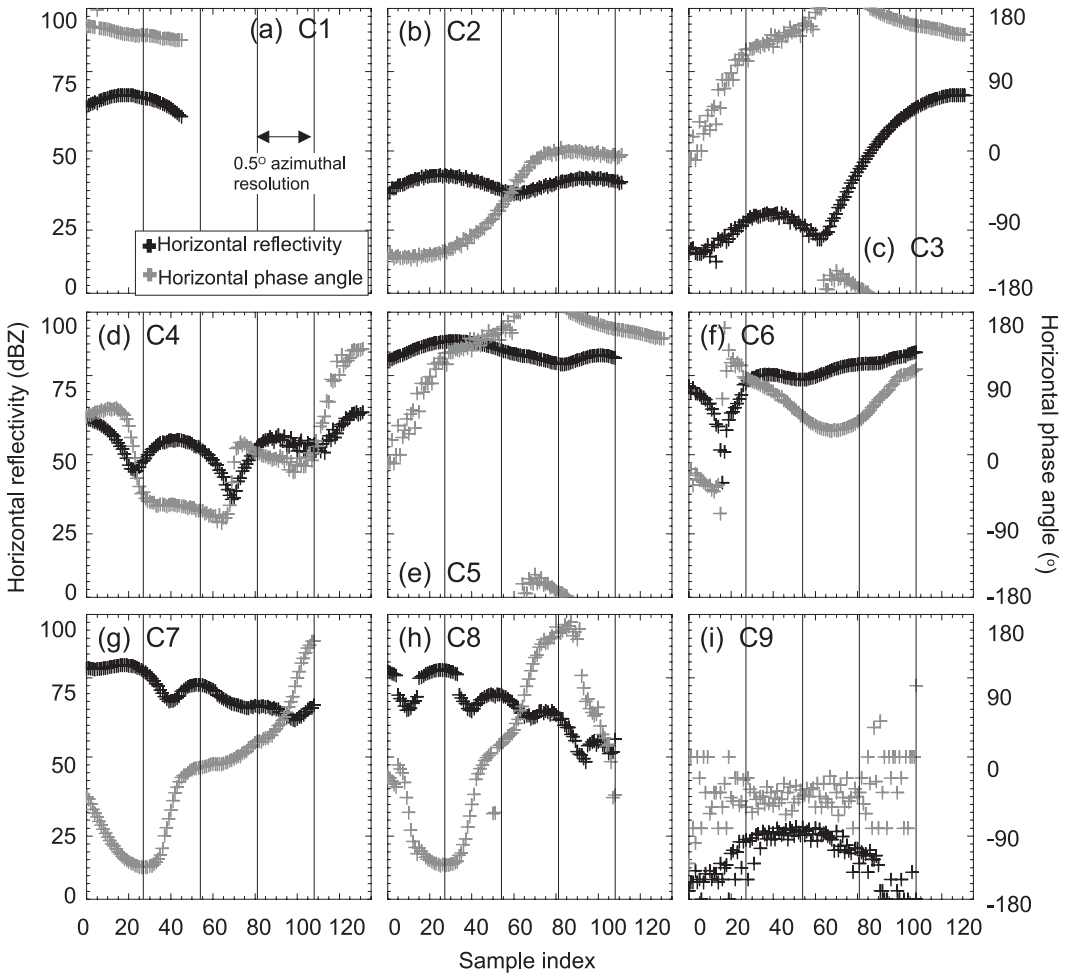

FIG. 3. Same as in Fig. 2, but showing horizontal reflectivity (black plus symbols) and phase angle (gray plus symbols) of nine urban obstacles denoted as (a)–(i) C1, C2, C3, . . . , C9, respectively. Radial position, azimuthal range, and mean values of the polarimetric quantities are listed in Table 2.

superposition of different targets were observed mainly in the vicinity of the radar (Figs. 3b,d,i). Position of the urban obstacles and average values of the polarimetric parameters are listed in Table 3. The nine ground clutter examples (denoted as C1–C9) were chosen for this analysis to be added to the eight reference precipitation fields (Table 2); the methodology is explained in more detail in section 3.

Small raindrops (<2 mm) are spherical particles becoming more oblate with increasing size. Because their radii are smaller than 0.07 of the transmitted wavelength, raindrops are considered Rayleigh scatterers. Urban obstacles and mountains are non-Rayleigh scatterers showing a very different scattering cross section for horizontally and vertically polarized radiation. Compared to precipitation, urban obstacles usually show random amplitudes and phases leading to low ρ_{hv} values, noisy ϕ_{dp} (Illingworth 2003), and positive and negative extremes of Z_{dr} (Hubbert and Bringi 2000). Nevertheless, not all of the mean polarimetric variables for ground clutter listed in Table 3 lay clearly outside the typical ranges for Z_h, Z_{dr}, ρ_{hv}, and ϕ_{dp} typically observed within precipitation at C-band frequency (e.g., Keenan 2003).

3. Methodology

a. Superposing I and Q samples of ground clutter on precipitation samples

To investigate the influence of urban obstacles on the precision of polarimetric radar parameter estimation, I and Q samples of urban obstacles are superimposed on those observed within precipitation (denoted as "Superposing I and Q samples" in Fig. 4). Nine samples of

TABLE 3. Radial position, azimuthal range (number of samples shown in brackets), and polarimetric characteristics such as horizontal reflectivity Z_h, differential reflectivity Z_{dr}, correlation coefficient ρ_{hv}, and differential propagation phase ϕ_{dp} for the nine urban obstacles used for the analysis. Horizontal reflectivity and phase angle for obstacles are shown in Fig. 3.

	Radial position (km)	Azimuthal range (°)	Z_h (dBZ)	Z_{dr} (dB)	ρ_{hv}	ϕ_{dp} (°)
C1	24.0	0.8 (46)	67.9	4.9	0.96	51.1
C2	20.9	2.1 (112)	39.2	−3.7	0.87	123.4
C3	24.0	2.4 (132)	61.6	7.3	0.96	56.8
C4	3.8	2.4 (132)	56.8	−4.4	0.30	43.4
C5	0.7	2.0 (109)	86.7	0.5	0.94	−5.9
C6	1.4	2.0 (109)	79.9	−3.2	0.91	132.8
C7	1.68	2.0 (109)	76.8	−0.9	0.53	−11.2
C8	1.92	2.0 (109)	73.9	−1.2	0.33	12.4
C9	23.8	2.0 (109)	19.6	5.3	0.81	126.1

urban obstacles (Table 3; Fig. 3) are superimposed on each of the eight precipitation fields (Table 2). Each I and Q clutter signatures having an azimuthal range of 0.8°(C1)–2.4° (C3, C4) were added continuously along the azimuth to the I and Q samples of the precipitation over the entire 360° azimuthal scan. The methodology is illustrated in Fig. 5 for 300 samples (~5.5° azimuthal interval) superimposing urban obstacles denoted as C1 and C3 (solid black lines) to those of precipitation observed at 1451 UTC 15 November 2005 (solid black lines). To investigate the sensitivity of polarimetric quantities to echoes from urban obstacles, the intensity of urban obstacles is modified in a way so that it is smaller, equal, and larger than that of precipitation. The intensity of the I and Q obstacle samples[1] were modified based on the horizontal reflectivity of precipitation according to the scaling factor $f(k)$, which is calculated as

$$f(k) = \sqrt{z_h^C \Big/ k\, z_h^P} = \sqrt{\sum\left[(I_h^C)^2 + (Q_h^C)^2\right] \Big/ k \sum\left[(I_h^P)^2 + (Q_h^P)^2\right]}, \quad (1)$$

with k being the scaling interval ranging from 0.001 (−30 dB) to 1000 (30 dB) with steps of $\Delta[10\log_{10}(k)] = 2$ dB. The mean horizontal reflectivity of precipitation (ground clutter) within the sample volume is denoted as $z_h^P(z_h^C)$ in units of mm^6 m^{-3} with I_h^P (I_h^C) being the in-phase and Q_h^P (Q_h^C) being the quadrature component of the complex signal within precipitation (ground clutter) at horizontal polarization.

[1] In the following, urban obstacles are also referred to clutter or ground clutter.

In Fig. 5 the intensity of urban obstacles was reduced so that the average horizontal reflectivity of ground clutter within a resolution volume (over 27 pulses) is equal to that of precipitation with $k = 1$ (dashed black lines). Then, intensity-scaled I and Q samples of urban obstacles [$I_h^{fC} = f(k)\, I_h^C, Q_h^{fC}, I_v^{fC}, Q_v^{fC}$; dashed black lines] were superimposed on I and Q samples of precipitation ($I_h^P, Q_h^P, I_v^P, Q_v^P$; thick solid black lines). With this technique, ground clutter intensity is adjusted to the precipitation intensity within each sample volume according to the horizontal reflectivity within the respective precipitation sample volume. Each I and Q clutter sample was added to the precipitation samples 30 times, according to Eq. (1) [$-30 \le 10\log_{10}(k) \le 30$ dB, $\Delta 10\log_{10}(k) = 2$ dB]. For each sample volume, the intensity of ground clutter was modified in a way so that its intensity is smaller than that of rain [$-30 \le 10\log_{10}(k) \le -2$ dB], equal to that of rain [$10\log_{10}(k) = 0$ dB], or larger than that of rain [$2 \le 10\log_{10}(k) \le 30$ dB].

b. Signal processing

The superposition of I and Q precipitation and ground clutter samples is accomplished on a pulse-by-pulse basis along the azimuth. The superimposed I and Q samples [e.g., $I_h^{PfC} = I_h^P + f(k)\, I_h^C$; solid gray lines in Fig. 5] were projected onto a polar grid with 0.5° azimuthal and 240-m-range resolution (thin vertical lines), and Z_h, Z_{dr}, ϕ_{dp}, and ρ_{hv} were derived (denoted as "Signal Processor" in Fig. 4). Note that the azimuthal range of the clutter signature that ranges from 45 to 119 samples always exceeds the azimuthal resolution of 27 samples, corresponding to 0.5° azimuthal resolution (Fig. 3). The latter approach was chosen to realistically simulate the effect of antenna side lobes hitting urban obstacles or mountains. The polarimetric parameters Z_h, Z_{dr}, ϕ_{dp}, and ρ_{hv} were derived for precipitation (hereafter "reference field") and superposition of intensity-scaled ground clutter on precipitation (hereafter "simulation fields"). The polarimetric parameters from the reference fields are indicated by superscript P (e.g., Z_h^P). The superposition of intensity-scaled ground clutter (fC) on precipitation (P) is indicated by superscript PfC (e.g., Z_h^{PfC}). Horizontal reflectivity of intensity-scaled ground clutter (Z_h^{fC}) is additionally derived to illustrate the ratio between ground clutter and precipitation intensities. For each I and Q sample measured at a distance r from the radar, Z_h^{fC} was calculated as

$$Z_h^{fC}(k) = 10\log_{10}\left\{\left[f(k)I_h^C\right]^2 + \left[f(k)Q_h^C\right]^2\right\} + 10\log_{10}(r^2). \quad (2)$$

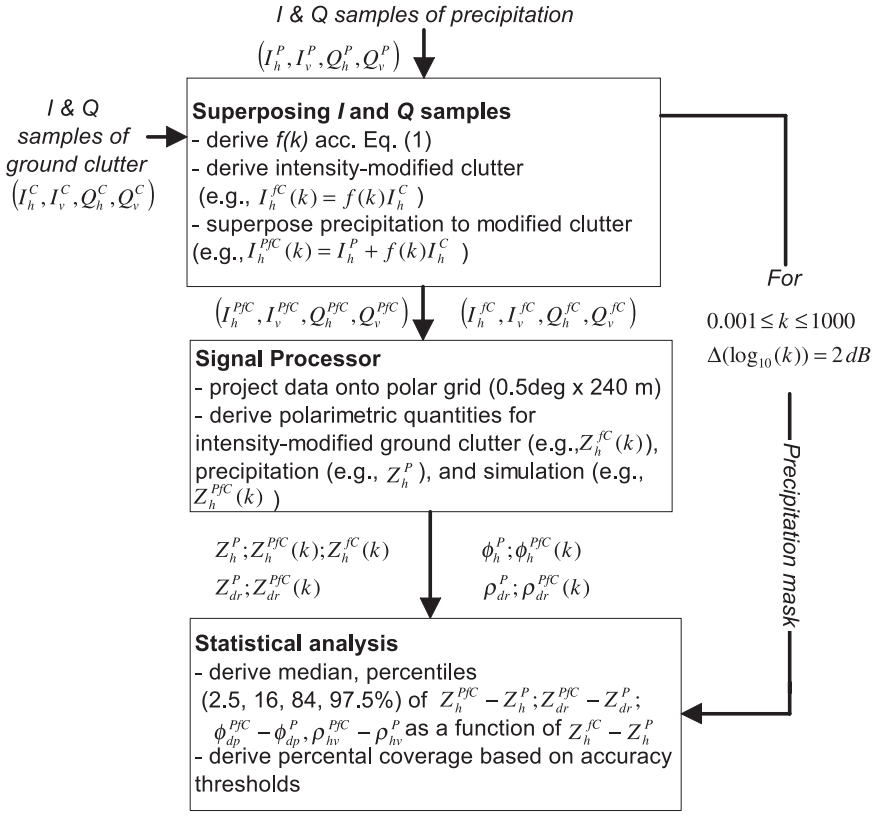

FIG. 4. Schematic showing the three steps of the data processing chain discussed in section 3.

Figures 5c,f shows horizontal reflectivity based on I and Q samples shown in Figs. 5a,b,d,e, respectively. While Fig. 5 illustrates the methodology for the simulation when the intensity of ground clutter is equal to the intensity of precipitation [$k = 1$ in Eq. (1)], Fig. 6 shows horizontal reflectivity of the superposition of intensity-scaled I and Q ground clutter samples on precipitation for $k = 0.001$, 10, and 1000 (Z_h^{PfC} in dBZ; solid gray lines). Horizontal reflectivity of the simulations was calculated as

$$Z_h^{\mathrm{PfC}}(k) = 10\log_{10}\left\{\left[I_h^P + f(k)I_h^C\right]^2 + \left[Q_h^P + f(k)Q_h^C\right]^2\right\} + 10\log_{10}(r^2). \quad (3)$$

In the same way, Z_{dr}, ϕ_{dp}, and ρ_{hv} were derived (Bringi and Chandrasekar 2001). Note that I_h^P (Q_h^P) and I_h^C (Q_h^C) can have a different sign that results in the downpointing spikes in Fig. 6. Due to the different signs of I and Q clutter and precipitation samples, the simulated reflectivity can also be smaller than the reference reflectivity for individual samples.

While Figs. 5, 6 illustrate the methodology for each individual I and Q sample, the projection of reference and simulation ($k = 10$) of Z_h, Z_{dr}, ρ_{hv}, and ϕ_{dp} onto a polar grid is shown in Fig. 7. Values of Z_{dr}, ϕ_{dp}, and ρ_{hv} showed a higher sensitivity to ground clutter, which will be further discussed in sections 4 and 5. Values became noisier with increasing ground clutter intensity. Differences between simulation and reference varied between about ±2 dB for Z_{dr} (cf. Figs. 7c,d), ±20° for ϕ_{dp} (cf. Figs. 7e,f), and ±0.2 for ρ_{hv} (cf. Figs. 7g,h). Spikes in radial direction evident in Figs. 7d,f,h are related to the way ground clutter was added to the reference field (i.e., periodically every 0.5°). The investigation area was limited to ranges of 100 km from the radar to assure a superior precision of the derived polarimetric variables. Effects of noise, miscalibration, and near-radome interference on the polarimetric quantities were removed or corrected.

c. Statistical analysis

The superposition of all nine ground clutter types with the eight precipitation events results in 8×9 simulations, each of them conducted for 30 ground clutter intensity classes. The clutter intensity classes

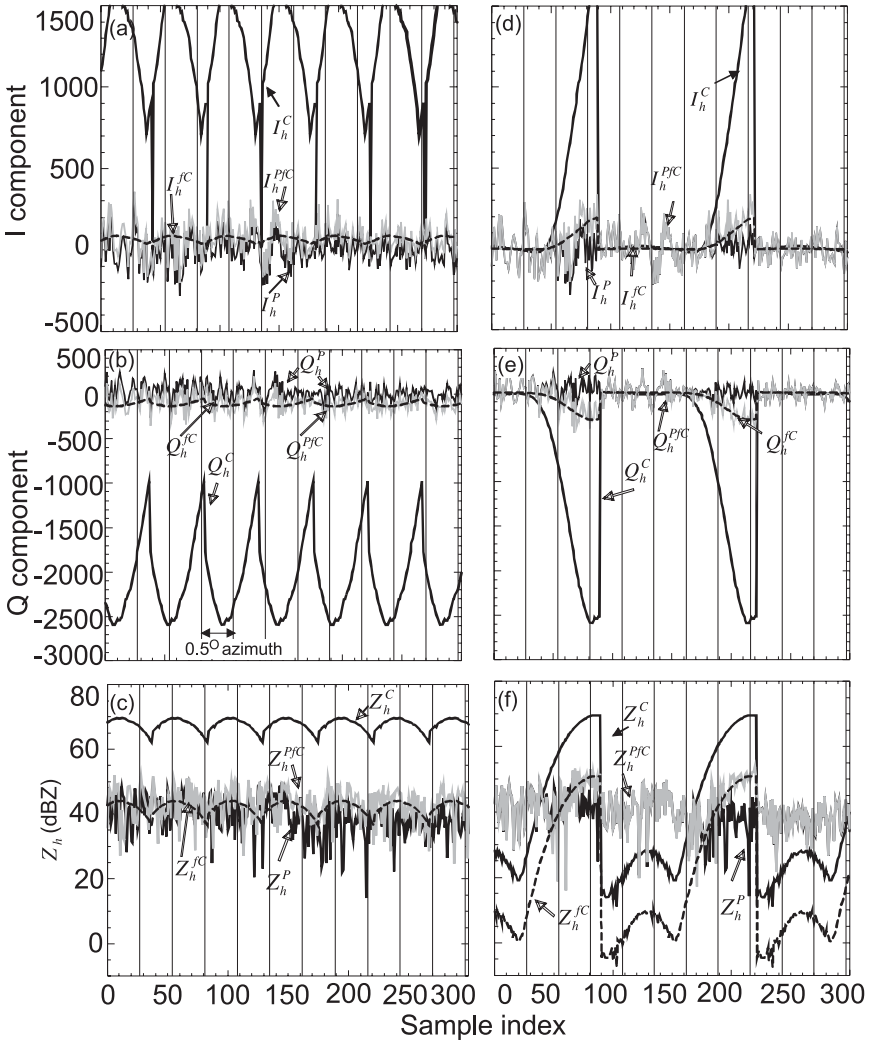

FIG. 5. Superposition of precipitation at 1451 UTC 15 Nov 2005 and ground clutter type (a)–(c) C1 and (d)–(f) C3. (a), (d) In-phase component (I_h); (b), (e) quadrature component (Q_h); and (c), (f) reflectivity at horizontal polarization (Z_h) are shown. Observed precipitation denoted as superscript *P* and ground clutter denoted as superscript *C* are indicated as solid black lines, respectively. Intensity-modified ground clutter [$k = 1$ in Eq. (1)] denoted as superscript fC is indicated as dashed black line. The superposition of precipitation and intensity-modified ground clutter denoted as superscript PfC is indicated as solid gray line.

ranged from −30 to 30 dB and were conducted in 2-dB intervals [according to Eq. (1)]. Because of the large amount of data per ground clutter intensity class (Table 4; 12 441 600 pixels), the analysis (denoted as ''Statistical analysis'' in Fig. 4) was divided in two parts. Analysis 1 (discussed in section 4a) focused on the sensitivity of the results to the precipitation event. In this case, the analysis was conducted for each precipitation event separately but combining all nine ground clutter types (analysis 1 in Table 4). With this approach, the focus was on determining the sensitivity of the result to the precipitation variation. Analysis 1 includes a maximum of $720 \times 240 \times 9$ (1 555 200) data pixels. In analysis 2 (discussed in section 4b), data were analyzed separately for each ground clutter type including all eight precipitation events. With this approach, the focus was on determining the sensitivity of the result to the ground clutter type. Analysis 2 includes a maximum of $720 \times 240 \times 8$ (1 382 400) data pixels per intensity level. The number of pixels for each ground clutter intensity class for analysis 1 after applying the precipitation thresholds (Table 1) is listed in Table 5. Analysis 2 includes 430 906 pixels for each ground clutter intensity class.

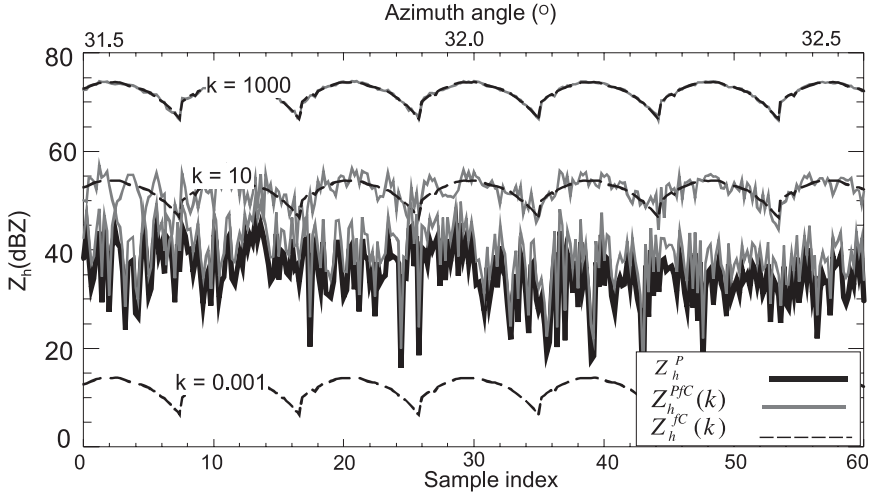

FIG. 6. Same as in Fig. 5c, but showing all intensity-modified ground clutter C1 for $k = 0.001$, 10, and 1000 [$Z_h^{\mathrm{fC}}(k)$; dashed black lines] and the superposition of precipitation and the intensity-modified ground clutter [$Z_h^{\mathrm{fC}}(k)$; solid gray lines]. Horizontal reflectivity of precipitation is denoted as Z_h^P and indicated as a solid black line.

In analyses 1 and 2, median and intervals in which 68% and 95% of the data are represented (16% and 84%; 2.5% and 97.5% bins, respectively) were calculated for each ground clutter intensity class. The calculation is based on the probability density function (PDF) of Z_h, Z_{dr}, $\rho_{\mathrm{h}\nu}$, and ϕ_{dp} derived from the differences between the precipitation–ground–clutter mixture and the reference precipitation field denoted as $Z_h^{\mathrm{PfC}} - Z_h^P$, $Z_{\mathrm{dr}}^{\mathrm{PfC}} - Z_{\mathrm{dr}}^P$, $\rho_{\mathrm{h}\nu}^{\mathrm{PfC}} - \rho_{\mathrm{h}\nu}^P$, and $\phi_{\mathrm{dp}}^{\mathrm{PfC}} - \phi_{\mathrm{dp}}^P$. For a standard normal PDF about 68% (95%) of the data is within 1 (2) standard deviation away from the mean. Figure 8 shows the difference between simulation and reference fields for Z_h, Z_{dr}, $\rho_{\mathrm{h}\nu}$, and ϕ_{dp} (y axis) for each resolution volume (thin gray line), medians (thick black lines), 16% and 84% bins (denoted as 68% data; thick, gray line) and 2.5% and 97.5% bins (denoted as 95% data; dashed, thick, gray line) for data obtained at 1451 UTC 15 November 2005. Data are presented as a function of ratio between ground clutter and precipitation intensity (x axis). Negative (positive) values of $Z_h^{\mathrm{fC}} - Z_h^P = 10\log_{10}(k)$ plotted along the x axis indicate that the scaled ground clutter intensity was smaller (larger) than that of precipitation.

Thresholds for polarimetric quantities are set to determine the critical level of ground clutter influence. The threshold for radar reflectivity is set to 1.7 dBZ, which is related to the overall uncertainty of a calibrated and maintained radar (Paul and Smith, 2001). For rainfall-rate estimation Illingworth (2003) showed that Z_{dr} needs to be measured with a precision of ~0.2 dB. Hubbert et al. (1993) and Keenan et al. (1998) showed that ϕ_{dp} can theoretically be measured with a precision of 3°. Segond et al. (2007) showed in a long-term analysis including data from almost 2 yr that $\rho_{\mathrm{h}\nu}$ varies between ±0.02 in areas without ground clutter contamination. These values serve as a precision threshold, indicating when the ground clutter intensity becomes critical to the measurement precision. Additionally, the amount of data in percent can be derived, which would meet the threshold as a function of ground clutter intensity.

4. Sensitivity of polarimetric parameters to ground clutter contamination

a. Analysis 1—Sensitivity to variation in precipitation

Figure 9 reveals the sensitivity of polarimetric parameters to variations in precipitation. The rain events are dominated by stratiform precipitation with low sensitivity in case-to-case variations in precipitation (Table 2). All ground clutter types are combined to analyze the ground clutter influence for each precipitation event separately. Ground clutter hardly influences the precision of horizontal reflectivity with medians of $Z_h^{\mathrm{PfC}} - Z_h^P < 0.5$ dB, as long as the precipitation intensity is much larger than the ground clutter intensity (up to $Z_h^{\mathrm{fC}} - Z_h^P = -5$ dB). The influence of ground clutter on the precision of Z_h increases ($Z_h^{\mathrm{PfC}} - Z_h^P > 1.7$ dB) when the ground clutter has the same intensity as precipitation. A standard deviation in the PDF of 1.7 dB (3.4 dB) for Z_h is reached when $Z_h^{\mathrm{fC}} - Z_h^P$ ranges between ±1 dB (±3 dB), as indicated by solid (dashed) gray lines in Fig. 9a. Results show a low sensitivity to the variation in precipitation with hardly any

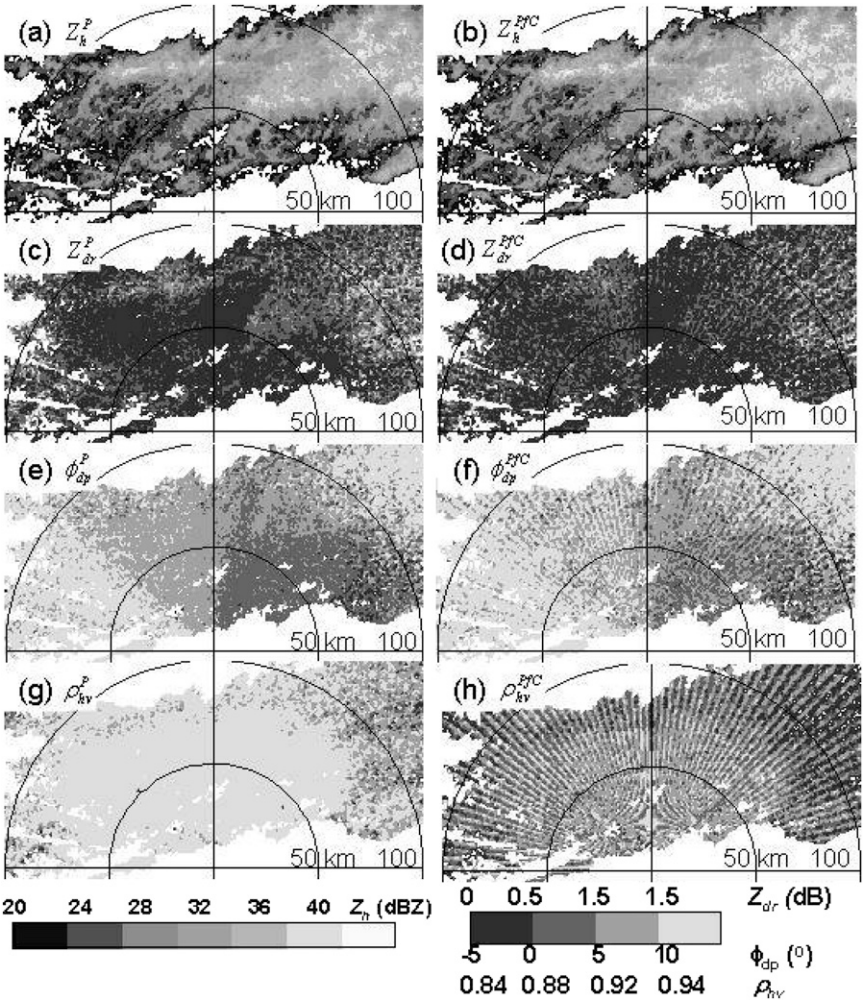

FIG. 7. (a), (b) Horizontal reflectivity (Z_h); (c), (d) differential reflectivity (Z_{dr}); (e), (f) differential propagation phase (ϕ_{dp}); and (g), (h) correlation coefficient (ρ_{hv}) at an elevation angle of 0.8° at 1451 UTC 15 Nov 2005. (left) Radar parameters of the reference precipitation fields denoted as superscript *P*. (right) Radar parameters of the simulation (denoted as superscript PfC) with a reflectivity of ground clutter being 10 dB*Z* higher than the precipitation reflectivity.

TABLE 4. List of the amount of data pixels. The analysis is conducted combining all precipitation events for each ground clutter type separately (denoted as analysis 1). analysis 2 was conducted combining all ground clutter types for each precipitation event. Maximum total number of pixels and the maximum number of pixels per intensity level for analysis 1 and analysis 2, respectively, are highlighted in italic.

Number of pixels in azimuth	720
Number of pixels in range	240
Analysis 1 (section 4a)	
Ground clutter samples	9
Number of pixels per clutter intensity level including all pixels in azimuth and range for all ground clutter samples	*720 × 240 × 9 (1 555 200)*
Analysis 2 (section 4b)	
Number of analysis times	8
Number of pixels per clutter intensity level including all pixels in azimuth and range for all precipitation events	720 × 240 × 8 (1 382 400)
Number of pixels per clutter intensity level including all pixels in azimuth and range for all ground clutter samples and analysis times	*720 × 240 × 9 × 8 (12 441 600)*

TABLE 5. Number of pixels per scan after applying thresholds in Table 1 for each analysis time and number of pixels per ground clutter intensity class included in analysis 1, derived by multiplying the number of pixels per scan by the number of ground clutter samples (9).

Analysis date	15 Nov 2005			2 Oct 2006	3 Oct 2006			
Analysis time (UTC)	1436	1446	1451	1226	0916	1226	1352	1356
Number of pixel after applying thresholds	63270	64959	65960	69264	37565	42607	45540	41741
Number of pixels for analysis 1	569430	584631	593640	623376	338085	383463	409860	375669

case-to-case variations, which is mainly related to the way precipitation and ground clutter are superimposed (section 3).

Differential reflectivity and differential phase measurements react differently to the ground clutter influence, showing both positive and negative differences between the simulation and the reference fields. As a result, the percentiles (gray lines in Fig. 9) indicate a large spread between simulation and reference fields (y axis), while the median values are close to zero. Small spread in percentiles and negative differences were observed for the correlation coefficient because ρ_{hv} within ground clutter is lower than within precipitation for the late autumn/early winter precipitation events. For this analysis, medians indicate that the precipitation intensity needs to be on average 1–3 dB for Z_{dr}, 4–7 dB for ϕ_{dp}, and 11–15 dB for ρ_{hv} higher than the clutter intensity to meet the precision thresholds. The influence of ground clutter is most pronounced for ρ_{hv} values. Because Z_{dr} and ϕ_{dp} of ground clutter is quite random compared to precipitation, the percentiles diverge quickly when the ground clutter influence increases

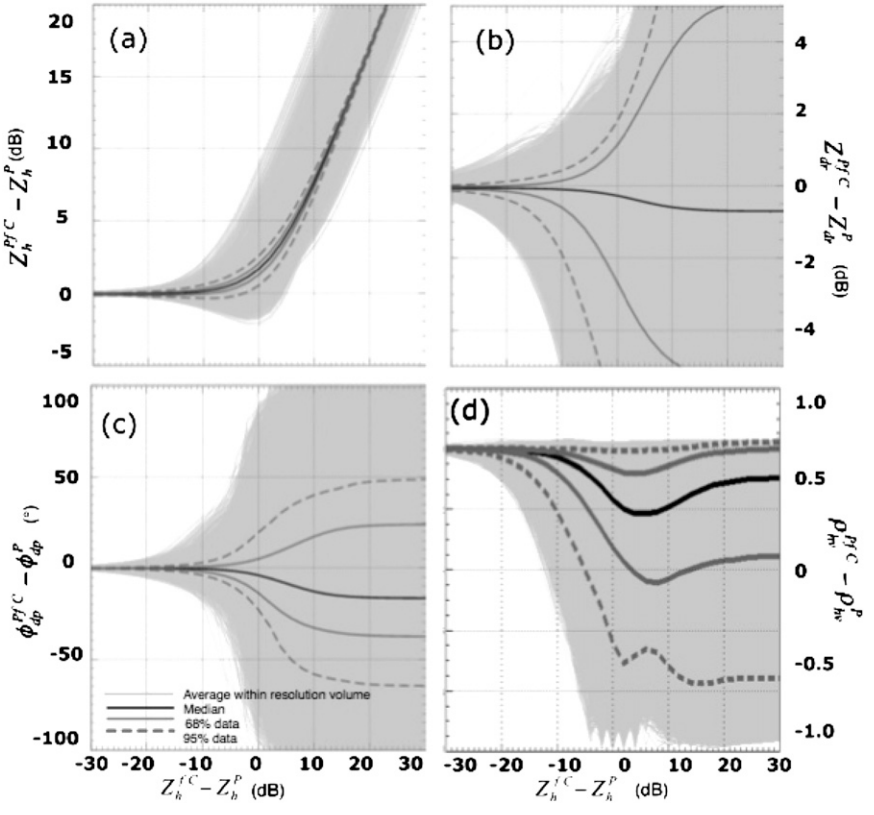

FIG. 8. (a) Horizontal reflectivity, (b) differential reflectivity, (c) correlation coefficient, and (d) differential phase of the simulations, including all resolution volumes combined with all nine ground clutter samples for data observed at 1451 UTC 15 Nov 2005. Each ground clutter intensity class with $\Delta\ (Z_h^{fC} - Z_h^P) = 2$ dB (x axis) includes 65 960 members. Each gray, thin line presents the average value within the resolution volume. Black, thick lines indicate median values; gray, thick lines indicate the 68% of the data; and dashed gray lines indicating 95% of the data.

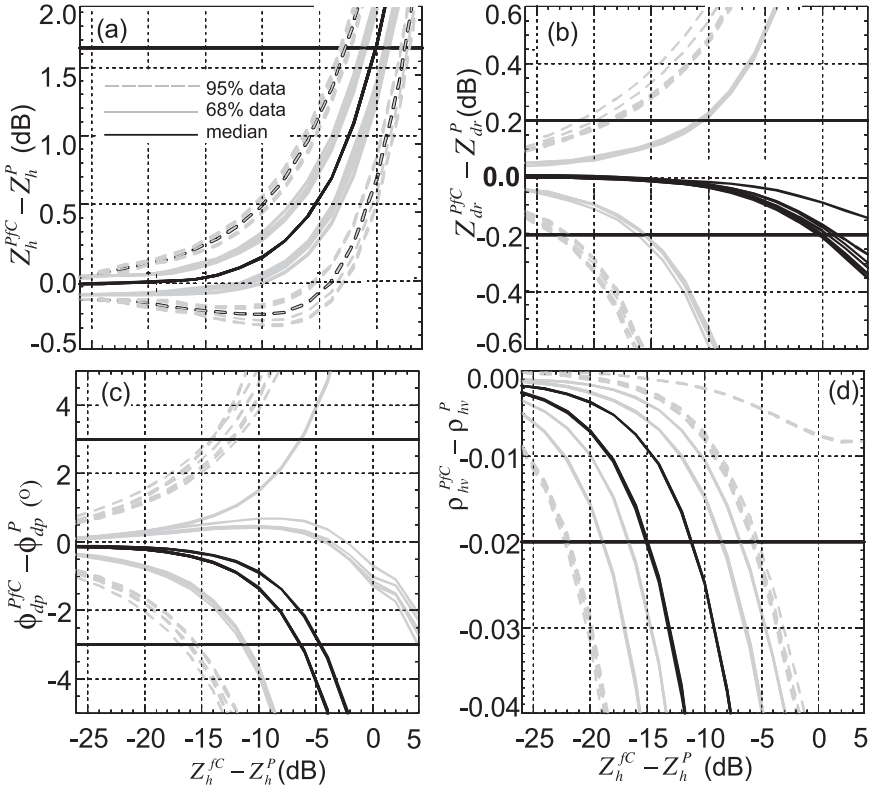

FIG. 9. Median (solid black lines), 68% of the data (solid gray lines), and 95% of the data (dashed gray lines) for (a) horizontal reflectivity, (b) differential reflectivity, (c) differential phase, and (d) correlation coefficient as a function of the difference between intensity-modified ground clutter and precipitation for all eight analysis times on 15 Nov and 2–3 Oct 2006, including all ground clutter types. The number of members per clutter intensity class is listed in Table 5. Precision thresholds are indicated as black horizontal lines.

($Z_h^{\mathrm{fC}} - Z_h^P > -15$ dB). The analysis further reveals that the standard deviation of the PDF is equal to the predefined precision threshold for Z_{dr} when the precipitation intensity is about 18 dB larger than the ground clutter intensity (solid gray lines intersecting the Z_{dr} threshold of 0.2 dB first at $Z_h^{\mathrm{fC}} - Z_h^P = -18$ dB in Fig. 9b). The standard deviation is twice the predefined threshold for Z_{dr} for the three precipitation events when the precipitation intensity is about 25 dB larger than the ground clutter intensity (dashed gray lines intersecting first at $Z_h^{\mathrm{fC}} - Z_h^P = -25$ dB in Fig. 9b). Applying the same analysis for ϕ_{dp} and ρ_{hv} in Figs. 9c,d reveals that precipitation intensity needs to be about 12 dB (17 dB) larger than the ground clutter intensity to have a standard deviation of the PDF, which is equal to (twice) the precision threshold for ϕ_{dp}, and about 19 dB (22 dB) larger for ρ_{hv}. The small spread between the medians (solid black lines in Fig. 9) might be linked to the low sensitivity to variations in precipitation from case to case. The spread of the median is less than 1° for ϕ_{dp}, which is 1/3 of the measurement precision and less than 0.02 for 0.02, which is the measurement precision. Because Z_{dr} is strongly dependent on drop size and shape, the largest variations from case to case occurred in the median (<0.4 dB being twice the measurement precision).

The amount of data that would meet the precision thresholds as a function of ground clutter intensity is shown in Fig. 10. The highest sensitivity to ground clutter was observed for Z_{dr} and ρ_{hv}. If 68% (95%) of the data is required to meet the precision thresholds, precipitation needs to be at least ~13.5 dB (22 dB) higher than the ground clutter for Z_{dr} and ~15 dB (20 dB) for ρ_{hv}. On the other hand, for accurate ϕ_{dp} measurement, precipitation is required to be ~9 dB (15 dB) higher than ground clutter to use 68% (95%) data.

b. Analysis 2—Sensitivity to ground clutter type

Polarimetric variables Z_{dr}, ϕ_{dp}, and ρ_{hv} are very sensitive to the ground clutter types C1–C9 as indicated by

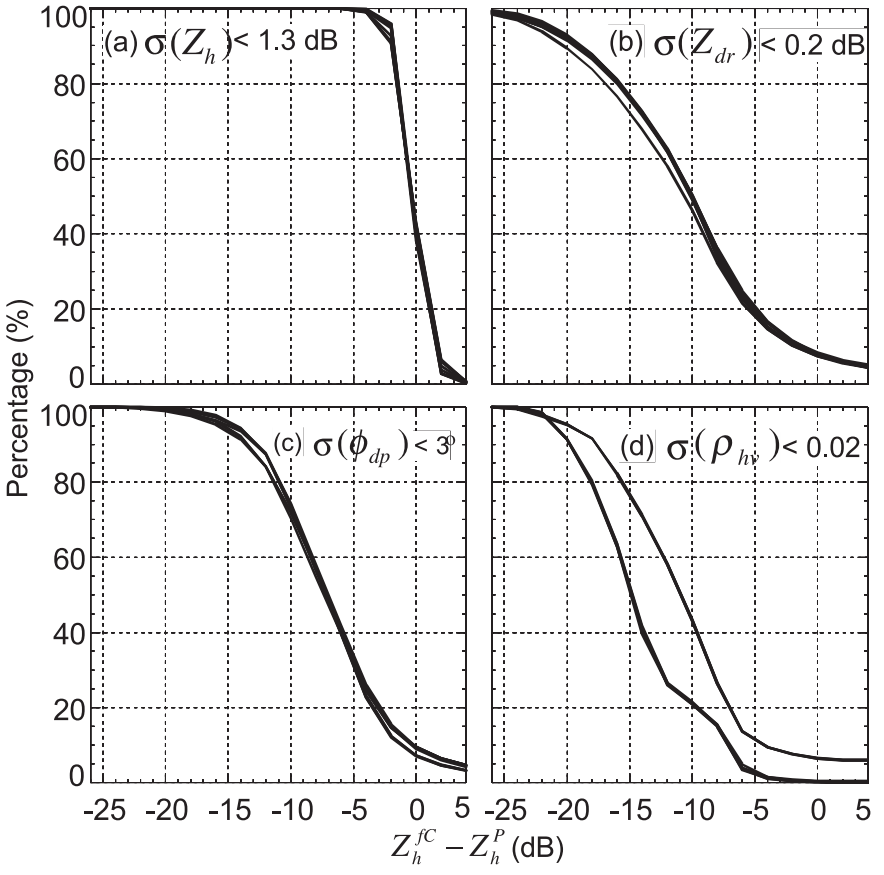

FIG. 10. Amount of data in percent for (a) Z_h, (b) $Z_{\rm dr}$, (c), $\phi_{\rm dp}$, and (d) $\rho_{\rm h\nu}$ that meets the predefined precision thresholds. The solid, black lines represent the eight analysis times on 15 Nov and 2–3 Oct 2006, including all ground clutter types.

median values in Fig. 11. Especially, $Z_{\rm dr}$ shows a random behavior with having both higher and lower values of $Z_{\rm dr}$ in ground clutter compared to precipitation, depending on the clutter type C1–C9. Although $\phi_{\rm dp}$ theoretically also has a random behavior, the results of this study imply that $\phi_{\rm dp}$ is less dependent on the ground clutter type compared to $Z_{\rm dr}$. For all simulations, the differential phase of precipitation exceeds that of the simulation. As already discussed, $\rho_{\rm h\nu}$ of urban obstacles is usually much lower than that of precipitation, which is reflected in Fig. 11d. Based on the simulations, ground clutter contamination is not critical for the measurement precision when precipitation is ~13 dB for $Z_{\rm dr}$, ~10 dB for $\phi_{\rm dp}$, and ~17 dB for $\rho_{\rm h\nu}$ larger than that of the ground values (medians in Fig. 11). Interestingly, some ground clutter types seem not to contaminate the polarimetric quantities of precipitation, such as C5 in Fig. 11b and C3 in Fig. 11c.

Simulations further indicate that the precipitation intensity needs to be on average 5–13 dB for $Z_{\rm dr}$, 2–10 dB for $\phi_{\rm dp}$, and 17–18 dB for $\rho_{\rm h\nu}$ higher than the precipitation to meet the precision thresholds (medians in Fig. 11). The standard deviation of the PDF is equal to (twice) the predefined precision thresholds when $Z_h^{\rm fC} - Z_h^P > -21$ dB (> -26 dB) for $Z_{\rm dr}$, $Z_h^{\rm fC} - Z_h^P > -13$ dB (> -18 dB) for $\phi_{\rm dp}$, and $Z_h^{\rm fC} - Z_h^P > -21$ dB (> -24 dB) for $\rho_{\rm hv}$ as indicated by the solid (dashed) thick gray lines in Figs. 11b–d. With respect to the amount of data meeting the predefined precision thresholds, precipitation intensity only needs to be ~1 and ~4 dB higher than the ground clutter intensity for Z_h as indicated in Fig. 12 to retrieve 68% and 95% of the data, respectively. According to the results of this study, the amount of data that can be retrieved in case of ground clutter contamination also strongly depends on the clutter type. Precipitation intensity only needs to be on average 6–13 dB (9–18 dB) higher than that of ground clutter to use 68% (95%) of the $\phi_{\rm dp}$ data. In the same context, the study reveals that precipitation needs to exceed ground clutter intensity by 8–18 dB (9–24 dB) to use $\rho_{\rm h\nu}$ values with a precision $\leq$0.02. Based on the superposition of urban obstacles C1–C9 and the three precipitation events close to Paris, the highest sensitivity for ground

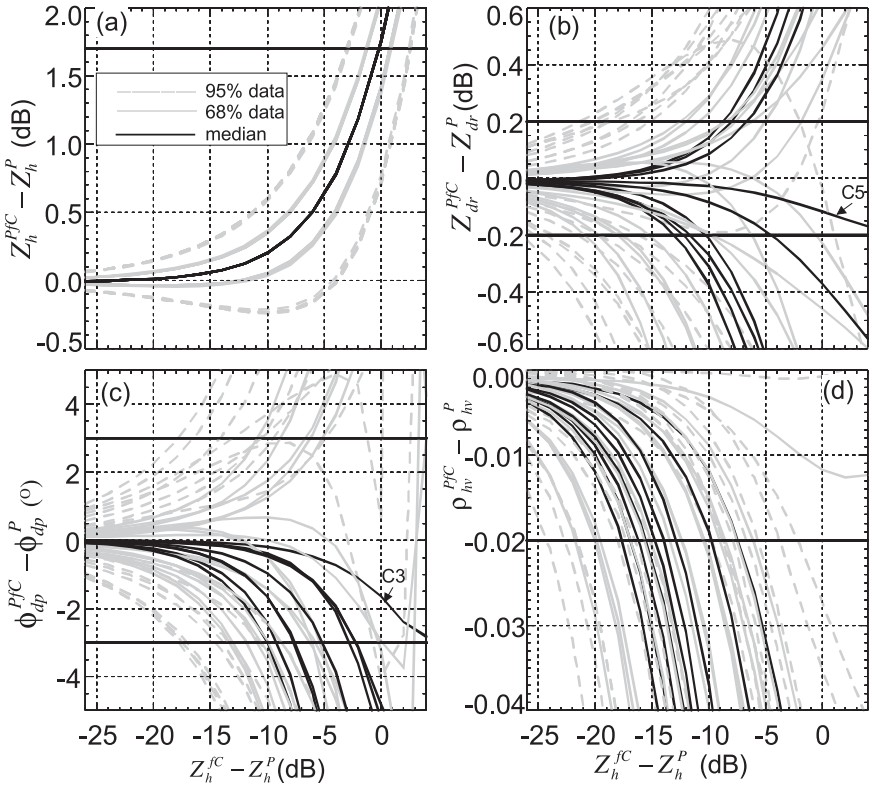

FIG. 11. Same as in Fig. 9, but showing median and percentiles of nine ground clutter types, including all precipitation events in the analysis. Median of ground clutter (b) type C5 is highlighted as is (c) type C3.

clutter was observed for Z_{dr}. Precipitation intensities should be on average 8–18 dB (15–25 dB) higher for a 68% (95%) data output.

5. Conclusions and outlook

The influence of ground clutter contamination on the estimation of polarimetric radar parameters, horizontal reflectivity (Z_h), differential reflectivity (Z_{dr}), correlation coefficient (ρ_{hv}), and differential propagation phase (ϕ_{dp}) were examined. For that purpose, nine spectral signatures from urban obstacles ranging from point targets (isolated buildings) to more complex signatures were superposed on precipitation fields. Because urban obstacles show similar backscattering characteristics as mountain ranges, it can be hypothesized that the results achieved in this study are applicable to mountainous and urban regions in a similar way. Structure and characteristics of the studied precipitation events are quite similar and represent typical midlatitude precipitation associated with warm- and cold-frontal rainbands in late autumn/early winter.

This study aimed to derive the critical level of ground clutter contamination for Z_h, Z_{dr}, ρ_{hv}, and ϕ_{dp} at which ground clutter influence exceeds predefined precision thresholds. Reference data with minimal ground clutter contamination consist of eight precipitation fields measured during three rain events. The nine ground clutter signatures were superimposed on each of the eight precipitation fields by scaling the ground clutter intensity from being 30 dB higher to 30 dB lower than the mean reflectivity of precipitation (with 2-dB steps). The resulting 30 ground clutter intensity classes are then analyzed with respect to sensitivity of the results to (i) the variation of precipitation by combining all ground clutter types for each precipitation event and (ii) the ground clutter type combining all precipitation events for each ground clutter type. To determine the critical level when the ground clutter influence becomes significant, precision thresholds are defined, which are set to 1.7 dB for Z_h, 0.2 dB for Z_{dr}, 3° for ϕ_{dp}, and 0.02 for ρ_{hv}.

Ground clutter has a strong influence on the precision of polarimetric quantities when its magnitude approaches that of precipitation. A precision of $Z_h < 1.7$ dB is achieved when the reflectivity of precipitation is at least 1 dB higher than that of ground clutter. Values of Z_{dr}, ρ_{hv}, and ϕ_{dp} are more sensitive to ground clutter

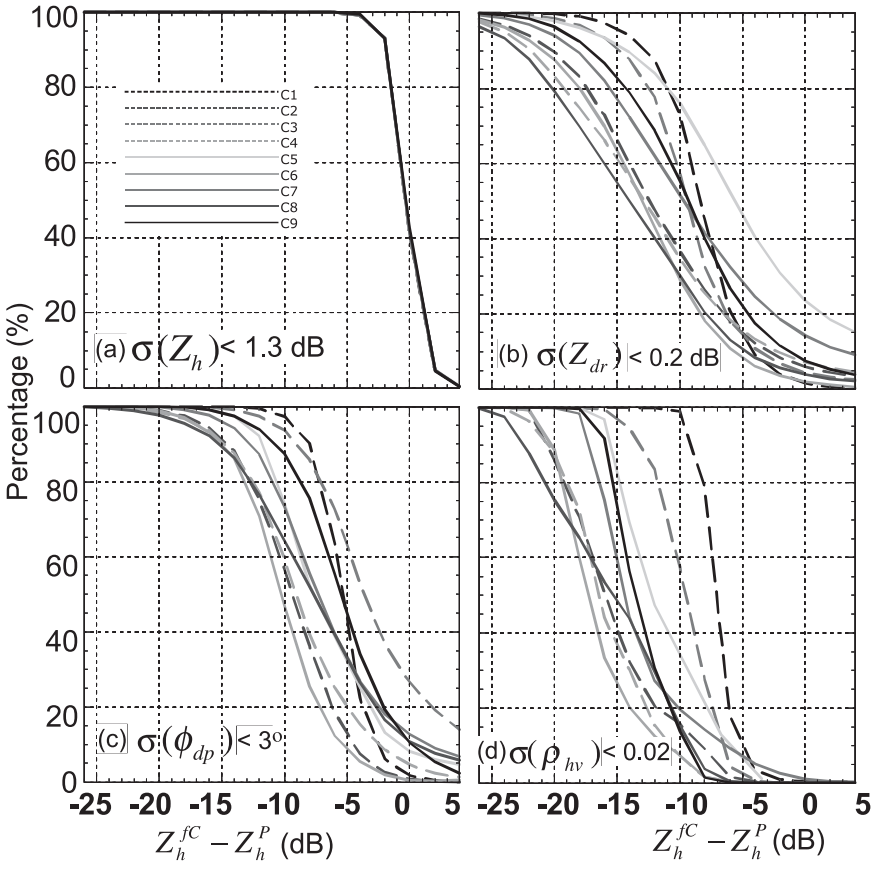

FIG. 12. Same as in Fig. 10, but showing the amount of data in percentage meeting the precision threshold for all nine ground clutter types indicated by different line styles and colors [scale in panel (a)].

influence even when the ground clutter intensity is *smaller* than the precipitation intensity. Figure 13 summarizes the results of this analysis. Ground clutter influence on the measurement precision strongly depends on the ground clutter type as shown by the error bars for analysis 2. Variation in the precipitation type has a minor impact (analysis 1). Highest sensitivity to both ground clutter and precipitation type was found for ρ_{hv}, while Z_{dr} shows a high sensitivity to the ground clutter type. Precipitation intensity needs to be on average 13.5 dB (ranging from 7–18 dB) higher than the ground clutter intensity for ρ_{hv} (square symbols in Fig. 13). For Z_{dr} and ϕ_{dp} (diamond and triangle symbols in Fig. 13), precipitation magnitude needs to be on average 2–9 dB and ~6 dB higher to achieve a precision of 0.2 dB and 3°, respectively.

How can the derived $Z_h^{fC} - Z_h^P$ values in Fig. 13 be applied to operational clutter filtering concepts in mountains where clutter recognition (remove clutter, obtain weather signal) is favored over clutter filtering and spatial interpolation? Clutter-to-signal ratios measured in real time can be compared to the estimated ratio for each precision threshold. In areas where the precipitation magnitude exceeds the values determined in this study, polarimetric quantities can be fully used for further applications. In areas where the precipitation magnitude is lower than the values derived in this study, conventional radar reflectivity is used or intensive clutter filtering techniques need to be applied specifically. The concept of using radar reflectivity when precision of polarimetric variables decreases can be applied right away. Ground clutter correcting for operational applications needs to be improved in the future to increase the spatial coverage of polarimetric measurements in mountainous terrain.

Analyzing the added benefit of polarimetry in the Swiss Alps, the size (number of pixels) affected by the derived critical level of $Z_h^{fC} - Z_h^P$ was derived for different precipitation intensities. This analysis is based on a worst-case scenario; that is, each bin is contaminated and no clutter filtering is applied. In an operational setting, intensive clutter filtering and identification will be applied. An example of how the spatial coverage for

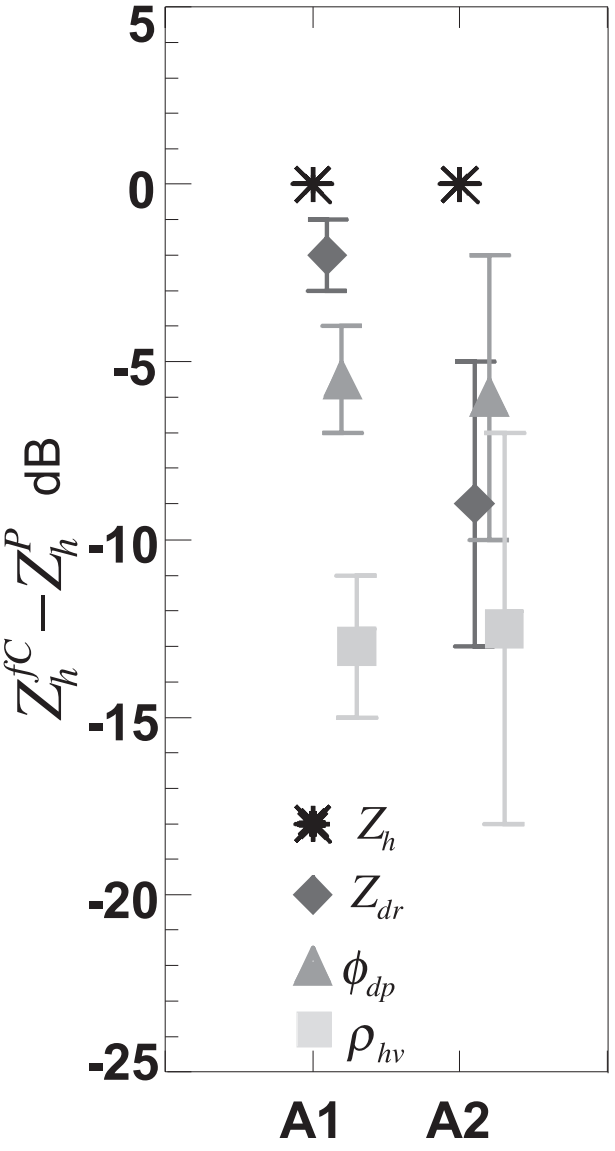

FIG. 13. Minimum and maximum values of $Z_h^{fC} - Z_h^P$ indicated by error bars and their mean indicated by the symbols for medians of analysis 1 (denoted as A1) and analysis 2 (denoted as A2). Star symbols represent Z_h, diamond symbols represent Z_{dr}, triangle symbols represent ϕ_{dp}, and square symbols represent ρ_{hv}.

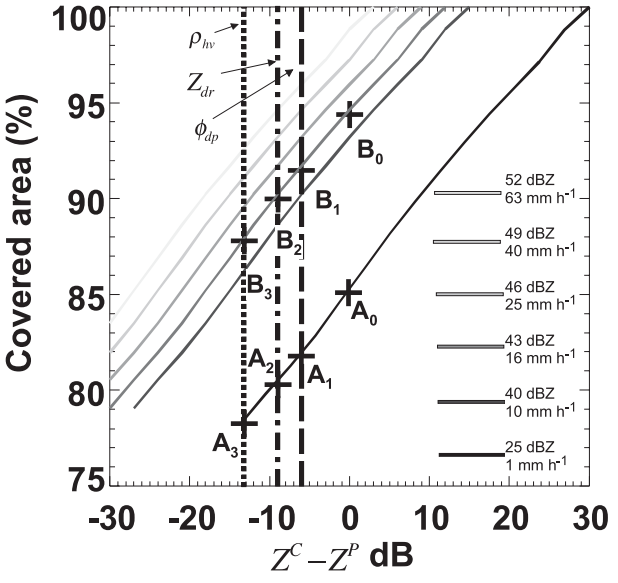

FIG. 14. Spatial coverage of the measurement domain obtained by the three Swiss weather radars as indicated in Fig. 1 as a function of $Z_h^C - Z_h^P$ for rainfall intensities indicated by gray lines ranging from 1 to 63 mm h^{-1}. To have the measurement precision, precipitation magnitude should exceed ground clutter magnitude by 6 dB as indicated as dashed line for ϕ_{dp}, 9 dB as indicated as dashed–dotted line for Z_{dr}, and 13 dB as indicated as dashed–dotted line for ρ_{hv}.

polarimetric parameters reduces if pixels contaminated by ground clutter are removed instead of corrected is given in Fig. 14. About 25% of the Swiss weather radar data is contaminated by ground clutter ($Z_h > 13$ dB in Fig. 1). The ratio between ground clutter derived from measurements within optical clear air (Z_h^C in Fig. 1) and predefined precipitation intensities is illustrated as a function of spatial coverage. Note that the spatial coverage is not reduced if we use conventional radar reflectivity. To derive the ground clutter–precipitation ratio, it is assumed that six precipitation fields (Z_h^P) with homogeneous rainfall rates passed over the measurement domain (indicated by gray lines in Fig. 14). If the rainfall rate is 1 mm h^{-1}, for example, in 85.5% of the area ground clutter and precipitation have the same intensity (indicated as A_0 in Fig. 14). When the rainfall rate increased to 16 mm h^{-1}, the spatial coverage increases to 94.5% (indicated as B_0 in Fig. 14). If now only those ϕ_{dp} values were considered where precipitation intensity is at least 6 dB higher than the ground clutter intensity, the spatial coverage decreases to 82% for 1 mm h^{-1} rainfall rate (point A_1) and 91.5% for 16 mm h^{-1} rainfall rate (point B_1). Applying the same idea for Z_{dr} where precipitation needs to be 9 dB higher to assure a precision of <0.2 dB, the spatial coverage decreased to 80.5% for 1 mm h^{-1} (point A_2) and 90% for 16 mm h^{-1} (point B_2). Because ρ_{hv} shows the highest sensitivity to ground clutter with a critical level of 13 dB, the spatial coverage decreased to 78.5% for 1 mm h^{-1} (point A_3) and 88% for 16 mm h^{-1} (point B_3).

The results show that algorithms able to identify and correct ground clutter are even more essential for polarimetric quantities than for reflectivity. Ground clutter can have a strong influence on the precision of polarimetric measurements even when its intensity is smaller than that of precipitation. Nevertheless, there are still large areas where ground clutter has little

influence on the precision of polarimetric parameters, making polarimetric radars a beneficial instrument for most applications in mountainous terrain. In those areas where the measurement precision of polarimetric parameters does not meet the predefined thresholds, conventional radar reflectivity can often be used. In the next step, investigations should focus on how sensitive polarimetric algorithms (e.g., used for particle identification, rainfall-rate estimation, attenuation corrects, and ground clutter identification) react to such influences to monitor the algorithm performance. The focus should be on analyzing to what degree ground clutter identification algorithms are able to eliminate the ground clutter contamination both using I and Q samples and processed data, especially when its intensity is much lower than that of rain and within areas with Doppler velocities close to zero. The investigation also revealed that ρ_{hv} is the parameter most sensitive to ground clutter contamination. This result is very important for polarimetric measurements within snow and hail, where values with $\rho_{hv} < 0.9$ can become comparable to those of urban obstacles and mountains. Future investigations will show whether ground clutter contamination is still detectable with conventional algorithms during precipitation events with snow, hail, and graupel.

Acknowledgments. We extend special thanks to Jacques Parent du Châtelet of Météo-France, Gianmario Galli, Bertrand Calpini of MeteoSwiss, and Martin Hagen of Deutsches Zentrum für Luft- und Raumfahrt, Oberpfaffenhofen, for many fruitful discussions regarding polarimetry. The authors thank Kim DoKhac of Météo-France for assisting in the acquisition of the radar data. Clarity and understanding of the analysis have been improved by many fruitful comments and suggestions made by the four anonymous reviewers to whom we also express our thanks. This research is part of the collaboration between Switzerland and France in the INTERREG IIIa project Radar de Franche-Comté. It is cofunded by the European Union, the French administration, Météo-France, MeteoSwiss, the Swiss State Secretariat for Economic Affairs, and the Swiss cantons Neuchâtel, Bern, Jura, Basel Landschaft, Fribourg, and Vaud.

REFERENCES

Blackman, M., and A. J. Illingworth, 1993: Differential phase measurement of precipitation. Preprints, *26th Conf. on Radar Meteorology*, Norman, OK, Amer. Meteor. Soc., 745–747.

Bringi, V. N., and V. Chandrasekar, 2001: *Polarimetric Doppler Weather Radar: Principles and Applications.* Cambridge University Press, 636 pp.

Doviak, R. J., and D. S. Zrnic, 1993: *Doppler Radar and Weather Observations.* Academic Press, 562 pp.

Friedrich, K., U. Germann, J. J. Gourley, and P. Tabary, 2007: Effects of radar beam shielding on rainfall estimation for polarimetric C-band radars. *J. Atmos. Oceanic Technol.,* **24,** 1839–1859.

Germann, U., G. Galli, M. Boscacci, and M. Bolliger, 2006: Radar precipitation measurement in a mountainous region. *Quart. J. Roy. Meteor. Soc.,* **132,** 1669–1692.

Giangrande, S. E., and A. V. Ryzhkov, 2005: Calibration of dual-polarization radar in the presence of partial beam blockage. *J. Atmos. Oceanic Technol.,* **22,** 1156–1166.

Gourley, J. J., P. Tabary, and J. Parent du Châtelet, 2007a: Empirical estimation of attenuation from differential propagation phase measurements at C band. *J. Appl. Meteor. Climatol.,* **46,** 306–317.

——, ——, and ——, 2007b: A fuzzy logic algorithm for the separation of precipitating from nonprecipitating echoes using polarimetric radar observations. *J. Atmos. Oceanic Technol.,* **24,** 1439–1451.

Hubbert, J., and V. N. Bringi, 2000: The effects of three-body scattering on differential reflectivity signatures. *J. Atmos. Oceanic Technol.,* **17,** 51–61.

——, V. Chandrasekar, V. N. Bringi, and P. Meischner, 1993: Processing and interpretation of coherent dual-polarized radar measurements. *J. Atmos. Oceanic Technol.,* **10,** 155–164.

Illingworth, A. J., 2003: Improved precipitation rates and data quality by using polarimetric measurements. *Weather Radar: Principles and Advanced Applications*, P. Meischner, Ed., Springer-Verlag, 130–166.

Joss, J., and R. Lee, 1995: The application of radar–gauge comparisons to operational precipitation profile corrections. *J. Appl. Meteor.,* **34,** 2612–2630.

Keenan, T. D., 2003: Hydrometeor classification with a C-band polarimetric radar. *Aust. Meteor. Mag.,* **52,** 23–31.

——, K. Glasson, F. Cummings, T. S. Bird, R. J. Keeler, and J. Lutz, 1998: The BMRC/NCAR C-band polarimetric (C-Pol) radar system. *J. Atmos. Oceanic Technol.,* **15,** 871–886.

Lee, R., G. Della Bruna, and J. Joss, 1995: Intensity of ground clutter and of echoes of anomalous propagation and its elimination. Preprints, *27th Conf. on Radar Meteorology,* Vail, CO, Amer. Meteor. Soc., 651–652.

Parent du Châtelet, J., P. Tabary, and M. Guimera, 2005: The PANTHERE Project and the evolution of the French operational radar network and products: Rain-estimation, Doppler winds, and dual-polarization. Preprints, *32nd Conf. on Radar Meteorology*, Albuquerque, NM, Amer. Meteor. Soc., 14R.6. [Available online at http://ams.confex.com/ams/pdfpapers/96217.pdf.]

Paul, J., and P. L. Smith, 2001: Summary of the radar calibration workshop. *Proc. 30th Conf. on Radar Meteorology*, Munich, Germany, Amer. Meteor. Soc., 174–176.

Segond, M.-L., P. Tabary, and J. Parent-du-Chatelet, 2007: Quantitative precipitation estimations from operational polarimetric radars for hydrological applications. Preprints, *33rd Conf. on Radar Meteorology*, Cairns, Australia, Amer. Meteor. Soc., 10.5. [Available online at http://ams.confex.com/ams/33Radar/techprogram/paper_123402.htm.]

Sugier, J., and P. Tabary, 2006: Evaluation of dual-polarisation technology at C-band for operational weather radar network. EUMETNET Opera 2 Rep., Work packages 1.4 and 1.5,

Deliverable b, 44 pp. [Available online at http://www.knmi.nl/opera.]

Tabary, P., 2007: The new French operational radar rainfall product. Part I: Methodology. *Wea. Forecasting,* **22,** 393–408.

——, J. Desplats, K. Do Khac, F. Eideliman, C. Gueguen, and J.-C. Heinrich, 2007: The new French operational radar rainfall product. Part II: Validation. *Wea. Forecasting,* **22,** 409–427.

Vivekanandan, J., D. N. Yates, and E. A. Brandes, 1999: The influence of terrain on rainfall estimation from radar reflectivity and specific propagation phase observations. *J. Atmos. Oceanic Technol.,* **16,** 837–845.

Zrnic, D. S., and A. V. Ryzhkov, 1996: Advantages of rain measurements using specific differential phase. *J. Atmos. Oceanic Technol.,* **13,** 454–464.

——, and ——, 1999: Polarimetry for weather surveillance radars. *Bull. Amer. Meteor. Soc.,* **80,** 389–406.